Text S1:

Ozone was selected instead of DSW as a photochemistry tracer for MLR, as it has previously been identified as a key oxidant for SOA formation by photochemistry at nearby Scripps Pier (Liu et al., 2011) and because there were fewer times when DSW was correlated to organic factors (Tables S6–S7). This selection increases the annual LO-OOA model R^2 by 11% with DSW explaining 16% but O_3 explaining 64% of the variability for LO-OOA predictions, while resulting in negligible differences for the other organic components (e.g. O/C and PMF factors). This result likely reflects the fact that ozone better represents cumulative photochemical reactions, whereas DSW is more reflective of the instantaneous reaction rates associated with local cloud attenuation. This distinction is particularly important at the coastal Mt. Soledad site, where persistent summer marine clouds suppress local solar radiation. As a result, ozone concentrations at Mt. Soledad decrease during summer relative to the nearby inland San Diego County Air Pollution Control District monitoring site at Kearny Mesa, which exhibits a clearer summer ozone maximum (Fig. S11) and a more pronounced daytime peak in ozone during summer (Fig. S12). Satellite-derived cloud fraction during summer was lower for the eastern region encompassing Kearny Mesa relative to the western offshore region adjacent to Mt. Soledad, consistent with less attenuation of solar radiation by clouds at the inland site and the corresponding higher ozone concentrations that were observed (Fig S11-12). Monthly correlations between the satellite-derived western cloud fraction and the local cloud fraction measured at Mt. Soledad were significant throughout the year (Table S16), suggesting that the satellite cloud fraction provides a reasonable proxy for local cloudiness at Mt. Soledad. In addition, correlations between satellite cloud fraction and PMF factors (Table S17) were similar to those obtained using local cloud fraction measurements from Total Sky Imager (Table S9), supporting the use of the satellite-derived cloud fraction to represent differences in cloud influence between the coastal and inland regions. Although odd oxygen (O_X = O_3 + NO_2) is commonly used as a photochemical tracer since O_X and OOA are produced from gas-phase oxidation of VOCs (Wood et al., 2010), NO_2 measurements were not available at Mt. Soledad or Scripps Pier. However, NO_2 measurements from the inland APCD Kearny Mesa monitoring site showed O_3 and O_X were strongly correlated (R = 0.87-0.94, Fig. S13). These results suggest that O_3 captures most of the variability in O_X, in part because NO_2 concentrations were small relative to ozone, making O_3 an appropriate photochemical tracer for the MLR analysis.

Table S1: Summary of studies investigating the combined effects of photochemical and aqueous-phase processing on oxidized organic aerosol.

Sampling Site	Organic Component	Photochemical Indicators	Aqueous Indicators	Citation
Beijing, China	MO-OOA	—	Positive correlation to nighttime ALWC, while LO-OOA has a negative correlation, suggesting aging of LO-OOA to MO-OOA.	Xiao et al. (2021)
Hong Kong	MO-OOA	Strong correlation to O_X (R^2 = 0.69).	Strong correlation to ALWC (R^2 = 0.26).	Yao et al. (2022)
Beijing, China	MO-OOA	Stronger correlation to Ox (R^2 = 0.46) than AWLC (R^2 = 0.15). Increased with O_X when O_X > 25 ppb.	Increased with ALWC when O_X < 35 ppb.	Zhan et al. (2021)
North China Plain	MO-OOA	Increased with O_X in spring/summer.	MO-OOA increased more rapidly than LO-OOA with RH (<90%) during winter/autumn.	Li et al. (2021)
Queens, NY	MO-OOA	ΔMO-OOA/ΔO_X increased by 24% when RH ≥ 65% compared to RH ≤ 55%.	—	Rogers et al. (2025)
Beijing, China	MO-OOA	Increased with O_X in autumn but remained relatively constant in summer.	Correlated with $C_2H_2O_2^+$, $C_2O_2^+$, and $CH_2O_2^+$. Increased from 20% to 40% as RH increased from 60% to >80%. Simultaneous decrease in LO-OOA during summer, suggesting aging of LO-OOA to MO-OOA.	Xu et al. (2017)
Yangtze River Delta, China	MO-OOA1	Daytime maximum; increase in mass fraction and concentration with O_X.	—	Huang et al. (2020)
Yangtze River Delta, China	MO-OOA2	Decreased with O_X.	Mass concentration increased with ALWC while mass fraction increased when ALWC <15 μg m^{-3}, well correlated with ALWC time series.	Huang et al. (2020)
Beijing, China	MO-OOA/ OA	—	Increased in mass fraction by 20 to 40% (from 0.8 to 1.0) as a function of RH and O_X, with minimal effects from O_X when RH is constant.	Xiao et al. (2021)
Hong Kong	MO-OOA/ LO-OOA	—	Increased with ALWC, suggesting aging from LO-OOA to MO-OOA.	Yao et al. (2022)
Beijing, China	LO-OOA	—	Stronger correlation with ALWC (R^2 = 0.54) than O_X (R^2 = 0.23).	Zhan et al. (2021)
Yangtze River Delta, China	LO-OOA	Increased with O_X during non-biomass burning periods.	Decreased with ALWC.	Huang et al. (2020)
North China Plain	LO-OOA	Increased with O_X in spring/summer.	LO-OOA increased with RH (<90%) during winter/autumn.	Li et al. (2021)
Beijing, China	LO-OOA	Stronger correlation to O_X than ALWC.	—	Xiao et al. (2021)
Beijing, China	LO-OOA	Increased with O_X across all seasons, with a rate higher than other factors during summer. Decreased or remained constant with RH.	—	Xu et al. (2017)

Table S1: continued.

Sampling Site	Organic Component	Photochemical Indicators	Aqueous Indicators	Citation
Queens, NY	LO-OOA	ΔLO-OOA/ΔOX increased by 69% when RH ≥ 65% compared to RH ≤ 55%.	Increased with RH at a greater rate than MO-OOA.	Rogers et al. (2025)
Pasadena, CA	SV-OOA	Daytime maximum.	—	Hayes et al. (2013)
Beijing, China	aq-OOA (OS fragments)	—	Mass fraction rapidly increased from RH 40 to 80%; High ALWC associated with high mass concentration.	Sun et al. (2016)
Mt. Hua, China	BSOA	—	pH strongly correlated with RH (R = 0.97) and ALWC (R = 0.80), reduced aerosol acidity suppressed the formation.	Li et al. (2013)
North Plain China	O/C	—	Increased with RH during all seasons except summer.	Li et al. (2021)
Beijing, China	O/C	—	Increased with ALWC at 50% < RH < 80%.	Sun et al. (2016)
Beijing, China	O/C	Increased with O_X during summer. Increased with O_X during autumn when O_X < 70 ppb, decreased when O_X > 70 ppb. Stayed constant with O_X during winter.	Increased from ~0.5 to ~0.7 as RH increased from 60% to 90% in autumn. Increased with RH during winter but not summer.	Xu et al. (2017)
Yangtze River Delta, China	O_{SC}	Increased with O_X.	Decreased with ALWC.	Huang et al. (2020)
Beijing, China	O/C_{SOA}	—	Increased by 20 to 40% (from 0.8 to 1.0) as a function of RH and O_X, with minimal effects from O_X when RH is constant.	Xiao et al. (2021)
Beijing, China	O/C_{SOA}	Decreased with O_X during summer. Increased with O_X during autumn when O_X < 70 ppb, decreased when O_X > 70 ppb. Stayed constant with O_X during winter.	Increased more rapidly at high RH levels than low RH levels.	Xu et al. (2017)
Yangtze River Delta, China	OA	Increased with O_X during non-biomass burning periods.	Increased with high ALWC during biomass burning periods.	Huang et al. (2020)

The abbreviations used in the table are as follows: RH – relative humidity, O_X – odd oxygen, O/C_{SOA} – oxygen-to-carbon ratio of secondary organic aerosol, O_{SC} – 2×O/C-H/C where H/C is the hydrogen-to-carbon ratio, aq-OOA – aqueous OOA, BSOA – biogenic SOA, BBOA – biomass burning OA, OS – organic sulfur.

Table S2: Summary of solutions and criteria used for PMF analysis of AMS NR HR-Org for ambient and CVI air masses. Criteria that are not applicable for one factor are indicated by N/A. Paired factors that do not have uncentered correlation coefficients (UC) higher than 0.8 are indicated by None.

Factor number (p) / Criteria	1	2	3	4	5	6	7	8
Q/Q_{exp}	2.87	1.23	2.03	1.91	1.83	1.79	1.75	1.73
Absolute residual	0.52	0.37	0.35	0.33	0.31	0.31	0.27	0.27
Temporal correlation factors strength (R > 0.8)	N/A	None	None	None	None	1 pair	2 pairs	3 pairs
Similarity of factor spectra (R > 0.8)	N/A	1 pair	3 pairs	5 pairs	8 pairs	6 pairs	3 pairs	4 pairs
Factors with less than 10% total mass	None	None	None	None	None	1 factor	3 factors	4 factors

Table S3: Annual average mass concentrations of AMS NR organic PMF factors at Mt. Soledad under ambient and CVI conditions, reported as mean ± standard deviation with median ± median absolute deviation (MAD) in brackets. Elemental ratios (O/C, S/C, N/C, H/C) are unitless. Mass concentrations are given in μg m^{-3}. All measurements exclude times with particle number concentrations exceeding 8000 cm^{-3}.

	Mass Concentration		Elemental Ratios			
PMF Factor	**Ambient**	**CVI**	**O/C**	**S/C**	**N/C**	**H/C**
SR-OOA	0.18 ± 0.21 [0.11 ± 0.16]	0.05 ± 0.06 [0.03 ± 0.05]	1.00	1.1×10^{-2}	1.3×10^{-2}	1.43
MO-OOA	0.78 ± 1.36 [0.40 ± 0.73]	0.15 ± 0.20 [0.07 ± 0.14]	1.47	1.6×10^{-4}	1.2×10^{-2}	1.01
LO-OOA	0.24 ± 0.45 [0.06 ± 0.27]	0.04 ± 0.07 [$(2 \pm 47) \times 10^{-3}$]	0.68	1.9×10^{-4}	4.3×10^{-3}	1.44
C-OOA	0.63 ± 0.90 [0.34 ± 0.61]	0.09 ± 0.14 [0.03 ± 0.10]	0.62	6.5×10^{-4}	1.7×10^{-2}	1.49
HOA	0.21 ± 0.34 [0.11 ± 0.19]	0.02 ± 0.06 [$(2 \pm 21) \times 10^{-3}$]	0.32	6.2×10^{-5}	2.4×10^{-3}	1.79

Table S4: Pearson correlation (R) coefficient values between AMS NR organic PMF factors and tracers at Mt. Soledad. All measurements exclude times with particle number concentrations exceeding 8000 cm^{-3}. Negative correlations are shaded blue and positive correlations are shaded red. The strength of each correlation determines the level of saturation for the corresponding shading- no correlation (|R| < 0.25)- white, weak correlation (0.25 ≤ |R| < 0.50)- light blue/red, moderate correlation (0.50 ≤ |R| < 0.80)- medium blue/red, strong correlation (0.80 ≤ |R|)- dark blue/red. Correlations that are statistically insignificant (p ≥ 0.05) are indicated by —.

	AMS NR Organic PMF Factors				
	SR-OOA	**MO-OOA**	**LO-OOA**	**C-OOA**	**HOA**
AMS NR Components					
Org	0.10	0.90	0.36	0.88	0.51
NO_3^-	—	0.33	0.52	0.56	0.46
SO_4^{2-}	0.84	0.43	-0.09	0.28	-0.01
NH_4^+	0.62	0.54	0.19	0.50	0.22
Chl^-	0.13	0.37	0.25	0.46	0.51
AMS NR Organic Elemental Ratios					
O/C	0.39	0.40	-0.27	0.06	-0.38
S/C	0.50	-0.24	-0.28	-0.36	-0.31
N/C	0.27	0.26	-0.41	0.40	-0.21
XRF					
V	—	—	—	—	—
Br	—	0.72	—	0.79	0.44
nss-K	—	0.44	—	0.55	—
Sea Salt	—	—	—	—	—
Dust	-0.27	—	—	0.33	—
Ti	—	—	—	0.35	—
Mn	—	—	—	—	0.31
Pb	—	—	—	—	0.33
Cu	-0.32	—	—	—	—
Zn	-0.30	—	—	—	—
Tracers					
Air Temperature	0.33	0.37	-0.07	0.44	0.03
Sea Surface Temperature	0.43	0.31	-0.24	0.30	-0.03
Wind Speed	-0.36	-0.22	-0.22	-0.20	-0.17
Wind Direction	0.18	0.10	0.13	—	-0.23
CPC Particle Number Conc.	-0.30	-0.04	0.36	0.28	0.49
CIMS HNCO	0.22	0.37	0.06	0.27	—
O_3	-0.13	0.15	0.37	0.10	-0.06
DSW	0.14	0.04	-0.01	0.11	-0.04
UCVF	0.52	0.11	-0.16	-0.10	-0.24
LCF	0.11	-0.01	-0.16	-0.07	-0.02
RH	0.33	0.05	-0.13	-0.13	-0.14
rBC	-0.06	0.12	0.06	0.33	0.28

Table S5: Pearson correlation (R) coefficient values between AMS NR organic PMF factors and FTIR NV organic functional groups and PMF factors above the detection limit (ADL) at Mt. Soledad. Values in brackets, [n], indicate the number of filters ADL. All measurements exclude times with particle number concentrations exceeding 8000 cm^{-3}. Negative correlations are shaded blue and positive correlations are shaded red. The strength of each correlation determines the level of saturation for the corresponding shading- no correlation ($|R| < 0.25$)- white, weak correlation ($0.25 \leq |R| < 0.50$)- light blue/red, moderate correlation ($0.50 \leq |R| < 0.80$)- medium blue/red, strong correlation ($0.80 \leq |R|$)- dark blue/red. Correlations that are statistically insignificant ($p \geq 0.05$) are indicated by —.

FTIR NV	AMS NR Organic PMF Factors				
	SR-OOA	MO-OOA	LO-OOA	C-OOA	HOA
Functional Groups (<1 µm) [n]					
Alcohol [242]	-0.25	0.31	—	0.37	0.33
Alkane [252]	0.37	0.40	—	0.42	0.27
Amine [218]	—	0.49	0.26	0.62	0.47
Acid [98]	0.64	0.55	—	0.28	—
Carbonyl [45]	—	0.78	—	0.62	0.51
Functional Groups (<0.5 µm) [n]					
Alcohol [92]	-0.23	0.49	—	0.51	0.46
Alkane [119]	—	0.63	—	0.71	0.51
Amine [93]	—	0.52	—	0.57	0.44
Acid [86]	—	0.26	0.25	0.56	0.22
Carbonyl [10]	—	0.85	—	0.78	—
Functional Groups (<0.18 µm) [n]					
Alcohol [161]	-0.23	0.34	—	0.43	0.52
Alkane [166]	-0.17	0.38	—	0.49	0.52
Amine [118]	-0.25	0.26	—	0.41	0.55
Acid [88]	-0.24	0.30	—	0.41	0.28
Carbonyl [12]	—	0.64	—	0.69	—
PMF Factors (<1 µm)					
Sulfate-Correlated (SC) [252]	0.56	—	—	—	—
Fossil Fuel (FF) [252]	0.33	0.40	0.14	0.39	0.23
Dust-Correlated (DC) [252]	-0.34	0.14	—	0.22	0.22
Biomass Burning (BB) [252]	—	0.68	0.31	0.71	0.44
NV Organics [n]					
<1 µm [252]	0.14	0.56	—	0.58	0.39
<0.5 µm [122]	—	0.70	—	0.74	0.51
<0.18 µm [171]	-0.21	0.45	—	0.55	0.54

Table S6: Pearson correlation (R) coefficient values between AMS NR organic PMF factors and O_3, DSW, UCVF, LCF, RH, and rBC at Mt. Soledad. All measurements exclude times with particle number concentrations exceeding 8000 cm^{-3}. Negative correlations are shaded blue and positive correlations are shaded red. The strength of each correlation determines the level of saturation for the corresponding shading- no correlation ($|R| < 0.25$)- white, weak correlation ($0.25 \leq |R| < 0.50$)- light blue/red, moderate correlation ($0.50 \leq |R| < 0.80$)- medium blue/red, strong correlation ($0.80 \leq |R|$)- dark blue/red. Correlations that are statistically insignificant ($p \geq 0.05$) are indicated by —.

		Jan	Feb	Mar	Apr	May	Jun	Jul	Aug	Sep	Oct	Nov	Dec
O_3	SR-OOA	—	0.18	0.22	-0.07	0.34	—	0.27	0.32	0.03	0.06	—	-0.04
	MO-OOA	0.76	0.12	0.36	0.58	0.43	0.47	0.50	0.73	0.48	0.75	0.58	0.48
	LO-OOA	0.29	0.19	—	0.41	0.24	0.23	0.14	0.20	0.35	0.56	0.35	0.39
	C-OOA	0.83	-0.16	—	0.11	—	0.05	0.17	0.33	0.48	0.50	0.32	0.04
DSW	SR-OOA	0.73	0.15	0.20	—	-0.14	—	—	—	—	—	—	—
	MO-OOA	—	—	0.30	—	—	—	0.20	0.16	—	0.14	—	—
	LO-OOA	—	—	0.17	0.25	—	—	0.20	0.19	0.29	0.23	0.37	0.20
	C-OOA	—	—	—	0.18	—	0.17	—	—	—	0.15	—	—
UCVF	SR-OOA	—	—	0.16	0.59	0.39	0.17	0.47	0.41	-0.38	0.23	0.42	0.52
	MO-OOA	—	—	—	0.39	0.66	0.17	0.38	0.25	-0.13	0.20	—	—
	LO-OOA	—	-0.16	—	-0.26	0.41	—	—	—	-0.19	—	—	-0.15
	C-OOA	-0.80	0.27	—	-0.34	0.23	-0.17	—	—	-0.29	—	—	-0.24
LCF	SR-OOA	—	—	—	0.39	0.22	-0.29	-0.14	-0.07	-0.18	0.10	—	—
	MO-OOA	—	-0.41	-0.34	0.25	0.41	—	0.09	-0.30	-0.10	—	—	-0.10
	LO-OOA	—	-0.15	-0.30	-0.35	0.31	0.18	0.13	-0.05	-0.11	-0.21	-0.21	-0.05
	C-OOA	—	-0.37	-0.18	-0.37	0.12	-0.16	0.05	-0.14	-0.07	-0.25	—	0.15
RH	SR-OOA	—	0.10	—	0.50	0.29	-0.19	0.10	—	-0.22	0.31	0.37	0.35
	MO-OOA	-0.82	0.08	-0.36	-0.04	0.37	-0.07	-0.12	-0.41	0.11	-0.12	-0.14	—
	LO-OOA	-0.36	-0.11	-0.29	-0.37	0.39	0.07	-0.08	-0.08	-0.13	-0.08	0.03	-0.06
	C-OOA	-0.90	0.16	-0.16	-0.29	—	-0.20	-0.08	-0.32	—	-0.20	-0.10	-0.08
rBC	SR-OOA	—	—	—	-0.17	0.07	0.06	-0.18	—	-0.18	-0.07	-0.10	—
	MO-OOA	0.34	0.32	0.21	0.24	0.18	0.15	0.15	0.23	0.22	0.09	0.16	0.07
	LO-OOA	—	0.49	0.37	0.49	0.34	0.09	0.14	0.22	0.27	0.12	0.07	0.12
	C-OOA	0.37	0.16	0.10	0.33	-0.07	0.29	0.32	0.37	0.35	0.20	0.44	0.51
	HOA	0.22	0.24	0.39	0.39	0.34	0.20	0.16	0.43	0.38	0.19	0.56	0.33

Table S7: Seasonal averages of meteorological and aerosol-related parameters at Mt. Soledad. Values are reported as mean ± standard deviation, with median ± median absolute deviation (MAD) shown in brackets. Units are as follows: O_3 (ppb), DSW (W m^{-2}), UCVF (unitless), LCF (unitless), RH (%), rBC (ng m^{-3}), and AMS NR organic PMF Factors (µg m^{-3}). Percentages reported beneath each AMS NR organic PMF factor represent the difference between the maximum and minimum hourly mean concentrations normalized by the corresponding seasonal mean concentration, with larger values indicating stronger diurnal variability. AMS NR organic PMF factors are restricted to ambient conditions. O_3, rBC, and AMS NR organic PMF Factors exclude times with particle number concentrations exceeding 8000 cm^{-3}.

	Season			
	Winter	**Spring**	**Summer**	**Fall**
Tracers				
O_3 (ppb)	36.6 ± 8.4 [36.9 ± 5.4]	39.1 ± 7.2 [38.2 ± 4.2]	31.4 ± 7.3 [31.5 ± 5.2]	38.5 ± 10.6 [37.4 ± 5.4]
DSW (W m^{-2})	155 ± 245 [0 ± 0]	213 ± 308 [31 ± 31]	235 ± 324 [27 ± 27]	152 ± 232 [0 ± 0]
UCVF	0.29 ± 0.12 [0.28 ± 0.07]	0.64 ± 0.24 [0.68 ± 0.21]	0.61 ± 0.20 [0.62 ± 0.13]	0.35 ± 0.18 [0.33 ± 0.13]
LCF	0.47 ± 0.41 [0.35 ± 0.32]	0.62 ± 0.42 [0.89 ± 0.11]	0.62 ± 0.40 [0.82 ± 0.18]	0.40 ± 0.39 [0.18 ± 0.16]
RH (%)	66.2 ± 16.7 [69.8 ± 10.5]	73.5 ± 10.8 [76.2 ± 5.9]	76.3 ± 8.6 [77.7 ± 6.0]	58.6 ± 24.8 [68.8 ± 14.0]
rBC (ng m^{-3})	48 ± 118 [14 ± 13]	23 ± 35 [14 ± 9]	57 ± 62 [40 ± 20]	89 ± 152 [55 ± 34]
AMS NR Organic PMF Factors				
SR-OOA (µg m^{-3})	0.06 ± 0.07 [0.03 ± 0.03] 80%	0.20 ± 0.14 [0.16 ± 0.08] 69%	0.38 ± 0.26 [0.31 ± 0.15] 86%	0.05 ± 0.09 [0.03 ± 0.03] 82%
MO-OOA (µg m^{-3})	0.18 ± 0.22 [0.10 ± 0.09] 65%	0.26 ± 0.23 [0.22 ± 0.17] 52%	1.77 ± 2.08 [1.10 ± 0.63] 31%	0.70 ± 0.88 [0.50 ± 0.28] 51%
LO-OOA (µg m^{-3})	0.40 ± 0.58 [0.18 ± 0.17] 74%	0.25 ± 0.49 [0.09 ± 0.09] 102%	0.12 ± 0.28 [0.00 ± 0.00] 185%	0.22 ± 0.41 [0.07 ± 0.07] 130%
C-OOA (µg m^{-3})	0.09 ± 0.23 [0.00 ± 0.00] 67%	0.10 ± 0.15 [0.01 ± 0.01] 72%	1.08 ± 1.03 [0.76 ± 0.35] 56%	1.07 ± 0.97 [0.81 ± 0.44] 39%
HOA (µg m^{-3})	0.26 ± 0.43 [0.13 ± 0.09] 115%	0.10 ± 0.22 [0.04 ± 0.04] 122%	0.23 ± 0.33 [0.12 ± 0.10] 130%	0.26 ± 0.35 [0.16 ± 0.12] 66%

Table S8: List of CIMS organic acid chemical names, formulas, abbreviations, and gas-phase mixing ratios reported in ppb as mean ± standard deviation and median ± median absolute deviation (MAD).

CIMS Organic Acids				
Chemical Name	**Chemical Formula**	**Chemical Abbreviation**	**Mean ± St. Dev. (ppb)**	**Median ± MAD (ppb)**
Acetic acid	$C_2H_4O_2$	AA	1.86 ± 1.05	1.69 ± 0.44
3-Butenoic acid	$C_4H_6O_2$	BEA	(2.60 ± 0.98) × 10^{-2}	(2.52 ± 0.62) × 10^{-2}
1,2,4-Butanetriol	$C_4H_{10}O_3$	BTL	(4.61 ± 4.49) × 10^{-5}	(3.45 ± 1.90) × 10^{-5}
Butyric acid	$C_4H_8O_2$	BUT	(6.39 ± 20.44) × 10^{-2}	(1.80 ± 1.43) × 10^{-2}
1-Cyclohexene-1-carboxylic acid	$C_7H_{10}O_2$	CHA	(1.30 ± 1.12) × 10^{-2}	(1.13 ± 0.34) × 10^{-2}
Cyanoacetic acid	$C_3H_3NO_2$	CYAA	(3.44 ± 1.94) × 10^{-4}	(3.13 ± 0.69) × 10^{-4}
Formic acid	CH_2O_2	FA	1.35 ± 1.06	1.11 ± 0.61
2-Furoic acid	$C_5H_4O_3$	FUA	4.82 ± 1.48	4.63 ± 0.85
Glycolic nitrile	C_2H_3NO	GAN	(4.42 ± 3.11) × 10^{-4}	(4.02 ± 1.97) × 10^{-4}
Glycolic acid	$C_2H_4O_3$	GLCA	(2.03 ± 1.58) × 10^{-2}	(1.57 ± 0.57) × 10^{-2}
Glyoxylic acid	$C_2H_2O_3$	GLYA	(1.46 ± 1.27) × 10^{-2}	(1.21 ± 0.56) × 10^{-2}
2-Hydroxybutyric acid	C_4H_8O3	HBA	(3.12 ± 1.84) × 10^{-3}	(2.62 ± 0.86) × 10^{-3}
2-Hydroxyisocaproic acid	$C_6H_{12}O_3$	HCA	(4.94 ± 2.33) × 10^{-4}	(4.37 ± 1.04) × 10^{-4}
2-Hydroxy-2-methylbutyric acid	$C_5H_{10}O_3$	HMBA	(2.73 ± 1.82) × 10^{-3}	(2.20 ± 0.86) × 10^{-3}
Nitrous Acid	HNO_2	HONO	(7.24 ± 4.96) × 10^{-2}	(5.56 ± 2.19) × 10^{-2}
Hexanoic acid	$C_6H_{12}O_2$	HEX	(1.32 ± 1.81) × 10^{-2}	(0.78 ± 0.63) × 10^{-2}
Ketobutyric acid	$C_4H_6O_3$	KBA	1.08 ± 1.01	0.83 ± 0.35
Lactic acid	$C_3H_6O_3$	LA	(1.81 ± 2.35) × 10^{-2}	(1.18 ± 0.75) × 10^{-2}
Levulinic acid	$C_5H_8O_3$	LVA	(1.95 ± 2.54) × 10^{-2}	(1.49 ± 0.54) × 10^{-2}
2-Nitroethanol	$C_2H_5NO_3$	NE	(4.79 ± 0.78) × 10^{-2}	(4.65 ± 0.46) × 10^{-2}
2-Octeneoic acid	$C_8H_{14}O_2$	OA	(5.39 ± 2.07) × 10^{-2}	(5.23 ± 1.43) × 10^{-2}
Propanoic acid	$C_3H_6O_2$	PA	2.88 ± 3.16	1.71 ± 1.52
2-Pentenoic acid	$C_5H_8O_2$	PEA	(1.62 ± 1.80) × 10^{-2}	(1.10 ± 0.58) × 10^{-2}
Pinonic acid	$C_{10}H_{16}O_3$	PINA	(1.95 ± 1.05) × 10^{-3}	(1.75 ± 0.41) × 10^{-3}
Propanetriol	$C_3H_8O_3$	PTL	(2.06 ± 1.89) × 10^{-2}	(1.68 ± 0.83) × 10^{-2}
Pyruvic acid	$C_3H_4O_3$	PYA	4.55 ± 2.78	(3.89 ± 1.25)
Valeric acid	$C_5H_{10}O_2$	VA	(2.22 ± 4.40) × 10^{-2}	(0.97 ± 0.77) × 10^{-2}

Table S9: Pearson correlation (R) coefficient values between AMS NR organic PMF factors and CIMS gas-phase organic acids at Mt. Soledad. All measurements exclude times with particle number concentrations exceeding 8000 cm^{-3}. Negative correlations are shaded blue and positive correlations are shaded red. The strength of each correlation determines the level of saturation for the corresponding shading- no correlation ($|R| < 0.25$)- white, weak correlation ($0.25 \leq |R| < 0.50$)- light blue/red, moderate correlation ($0.50 \leq |R| < 0.80$)- medium blue/red, strong correlation ($0.80 \leq |R|$)- dark blue/red. Correlations that are statistically insignificant ($p \geq 0.05$) are indicated by —.

	CIMS Gas-Phase Organic Acid Correlation of AMS NR Organic PMF Factors				
Chemical Abbreviation	**SR-OOA**	**MO-OOA**	**LO-OOA**	**C-OOA**	**HOA**
AA	0.12	0.12	0.37	0.10	0.06
BEA	0.33	0.32	-0.11	0.41	0.08
BTL	0.12	0.21	0.04	0.26	0.06
BUT	0.08	0.04	0.29	-0.16	—
CHA	0.10	0.04	0.10	—	0.09
CYAA	0.19	0.16	0.38	-0.09	0.12
FA	0.22	0.33	0.12	0.38	0.07
FUA	0.24	0.14	0.09	0.30	0.15
GAN	0.28	0.42	0.04	0.46	0.15
GLCA	0.29	0.43	0.51	0.16	0.13
GLYA	0.39	0.58	0.40	0.30	0.09
HBA	0.25	0.50	0.16	0.49	0.03
HCA	0.07	0.21	0.33	0.23	0.14
HMBA	0.20	0.38	0.03	0.40	-0.02
HONO	0.18	0.25	—	0.35	0.14
HEX	—	-0.07	0.32	-0.12	0.03
KBA	0.20	0.47	0.20	0.37	0.05
LA	0.12	0.08	0.21	—	0.10
LVA	0.16	0.39	0.23	0.28	0.05
NE	0.06	-0.03	0.23	-0.15	-0.04
OA	0.17	0.04	-0.04	0.11	0.07
PA	0.06	-0.15	0.12	-0.11	0.12
PEA	0.04	-0.13	0.20	-0.17	0.08
PINA	0.06	0.16	0.19	0.32	0.24
PTL	0.14	0.03	0.26	—	0.12
PYA	0.10	0.21	0.33	0.14	—
VA	0.07	—	0.38	-0.14	0.08

Table S10: Pearson correlation (R) coefficient values between CIMS gas-phase organic acids and processing tracers including O_3, DSW, UCVF, LCF, RH, rBC, and temperature at Mt. Soledad. Negative correlations are shaded blue and positive correlations are shaded red. The strength of each correlation determines the level of saturation for the corresponding shading- no correlation ($|R| < 0.25$)- white, weak correlation ($0.25 \leq |R| < 0.50$)- light blue/red, moderate correlation ($0.50 \leq |R| < 0.80$)- medium blue/red, strong correlation ($0.80 \leq |R|$)- dark blue/red. Correlations that are statistically insignificant ($p \geq 0.05$) are indicated by —.

	CIMS Gas-Phase Organic Acid Correlation of Processing Tracers						
Chemical Abbreviation	**O_3**	**DSW**	**UCVF**	**LCF**	**RH**	**rBC**	**Temp.**
AA	0.19	0.10	—	0.03	-0.08	0.11	0.04
BEA	-0.13	0.16	—	-0.14	—	0.09	0.28
BTL	0.17	0.36	0.10	-0.07	-0.24	0.16	0.45
BUT	0.17	—	0.13	0.08	—	—	-0.10
CHA	0.06	0.03	—	0.03	0.03	0.07	-0.09
CYAA	0.28	0.11	0.29	0.20	0.10	0.10	-0.02
FA	0.19	0.52	0.11	-0.21	-0.32	0.18	0.48
FUA	-0.07	—	—	-0.10	—	0.14	-0.02
GAN	—	0.24	0.28	-0.03	-0.15	0.27	0.33
GLCA	0.35	0.09	0.45	0.26	0.23	0.29	0.17
GLYA	0.27	—	0.43	0.25	0.23	0.26	0.13
HBA	0.26	0.40	0.30	0.08	-0.09	0.26	0.54
HCA	0.20	0.30	0.20	0.14	-0.11	0.29	0.26
HMBA	0.18	0.51	0.19	-0.06	-0.15	0.13	0.67
HONO	-0.05	0.52	0.10	-0.17	-0.27	0.20	0.57
HEX	0.16	-0.05	—	—	0.05	0.08	-0.14
KBA	0.23	0.39	0.26	0.04	-0.11	0.22	0.53
LA	0.15	0.10	0.21	0.16	0.06	0.13	-0.08
LVA	0.18	0.19	0.22	0.09	—	0.17	0.29
NE	0.72	0.19	-0.17	-0.04	-0.34	—	-0.14
OA	-0.04	—	-0.10	-0.03	0.02	—	—
PA	—	0.16	-0.28	-0.18	-0.20	-0.06	-0.18
PEA	0.15	0.14	-0.19	-0.15	-0.14	-0.02	-0.24
PINA	-0.17	0.05	0.10	0.10	0.09	0.32	0.02
PTL	0.16	0.29	0.10	-0.05	-0.13	0.08	0.18
PYA	0.28	0.42	—	—	-0.27	0.13	0.41
VA	0.34	-0.07	—	0.10	0.12	0.04	-0.20

Table S11: Pearson correlation (R) coefficient values between UCVF, LCF, and satellite cloud fraction (SCF) for each month. Negative correlations are shaded blue and positive correlations are shaded red. The strength of each correlation determines the level of saturation for the corresponding shading- no correlation (|R| < 0.25)- white, weak correlation (0.25 ≤ |R| < 0.50)- light blue/red, moderate correlation (0.50 ≤ |R| < 0.80)- medium blue/red, strong correlation (0.80 ≤ |R|)- dark blue/red. Correlations that are statistically insignificant (p ≥ 0.05) are indicated by —.

	Correlations of Cloud Fraction Measurements	
Months	**UCVF vs SCF**	**LCF vs SCF**
Jan	0.25	0.59
Feb	—	0.56
Mar	—	0.67
Apr	0.76	0.87
May	0.72	0.85
Jun	0.40	0.87
Jul	0.27	0.55
Aug	0.47	0.73
Sep	0.54	0.76
Oct	0.51	0.80
Nov	0.23	0.40
Dec	0.20	0.34

Table S12: Pearson correlation (R) coefficient values between AMS NR organic PMF factors at Mt. Soledad and satellite cloud fraction (SCF) at Scripps Pier. All measurements exclude times with particle number concentrations exceeding 8000 cm^{-3}. Negative correlations are shaded blue and positive correlations are shaded red. The strength of each correlation determines the level of saturation for the corresponding shading- no correlation ($|R| < 0.25$)- white, weak correlation ($0.25 \leq |R| < 0.50$)- light blue/red, moderate correlation ($0.50 \leq |R| < 0.80$)- medium blue/red, strong correlation ($0.80 \leq |R|$)- dark blue/red. Correlations that are statistically insignificant ($p \geq 0.05$) are indicated by —.

	SCF Correlation of AMS NR Organic PMF Factors			
Months	**SR-OOA**	**MO-OOA**	**LO-OOA**	**C-OOA**
Jan	—	—	—	—
Feb	0.28	-0.34	-0.23	-0.30
Mar	—	-0.26	-0.28	-0.23
Apr	0.50	0.27	-0.31	-0.34
May	0.22	0.40	0.33	0.13
Jun	-0.14	0.13	0.17	-0.12
Jul	—	0.11	0.12	0.16
Aug	—	-0.23	-0.16	-0.24
Sep	-0.10	-0.15	-0.17	-0.18
Oct	0.22	0.12	—	-0.10
Nov	0.23	-0.08	-0.09	—
Dec	0.27	-0.11	-0.23	-0.16

Table S13: Pearson correlation (R) coefficient values between AMS NR organic PMF factors and oxidation tracers (O_3, DSW, UCVF, LCF, and RH) and a mixed combustion tracer (rBC) at Mt. Soledad. All measurements exclude times with particle number concentrations exceeding 8000 cm^{-3}. Negative correlations are shaded blue and positive correlations are shaded red. The strength of each correlation determines the level of saturation for the corresponding shading- no correlation ($|R| < 0.25$)- white, weak correlation ($0.25 \leq |R| < 0.50$)- light blue/red, moderate correlation ($0.50 \leq |R| < 0.80$)- medium blue/red, strong correlation ($0.80 \leq |R|$)- dark blue/red. Correlations that are statistically insignificant ($p \geq 0.05$) are indicated by —.

Tracer \ PMF Factor	SR-OOA	MO-OOA	LO-OOA	C-OOA	HOA
O_3					
Winter	0.23	0.23	0.06	-0.09	-0.20
Spring	—	0.25	0.55	-0.28	0.16
Summer	0.13	0.46	0.27	0.40	—
Fall	—	0.58	0.43	0.32	-0.10
DSW					
Winter	0.19	0.14	0.12	—	—
Spring	—	—	0.12	0.11	—
Summer	0.10	—	0.15	—	-0.08
Fall	0.11	0.13	0.28	—	—
UCVF					
Winter	0.25	—	—	—	—
Spring	0.39	0.45	-0.23	—	-0.27
Summer	0.31	-0.09	-0.20	-0.22	-0.19
Fall	0.40	0.11	—	-0.12	-0.29
LCF					
Winter	0.10	-0.36	-0.20	-0.28	—
Spring	0.09	0.19	-0.16	-0.13	-0.16
Summer	-0.08	-0.11	-0.06	-0.08	0.04
Fall	0.07	-0.03	-0.13	—	0.16
RH					
Winter	0.15	-0.18	-0.16	-0.04	-0.04
Spring	0.29	—	-0.36	0.00	-0.25
Summer	-0.02	-0.04	-0.09	-0.10	-0.04
Fall	0.36	-0.09	0.03	-0.14	-0.13
rBC					
Winter	-0.19	0.28	0.17	0.27	0.09
Spring	—	0.15	0.18	0.08	0.22
Summer	-0.10	0.14	0.19	0.27	0.29
Fall	-0.11	0.10	0.09	0.34	0.43

Table S14: Multivariate linear regression (MLR) results showing normalized absolute and relative predictor contributions to predicted PMF factor mass concentrations (SR-OOA, MO-OOA, LO-OOA, C-OOA) and bulk O/C at Mt. Soledad for summer after excluding the September wildfire period. Predictor variables include ozone (O_3), upwind cloud volume fraction (UCVF), relative humidity (RH), refractory black carbon (rBC), and local cloud fraction (LCF). Values are reported as $m_i\bar{X}_{norm,i}$ with relative contributions (%) given in parentheses, calculated as the fractional contribution of each predictor to the sum of absolute contributions. Model performance is evaluated using uncentered coefficient of determination (R^2) and root mean square error (RMSE).

Predicted Variable	Ozone	UCVF	RH	rBC	LCF	R^2	RSME
O/C	0.33 (32%)	0.09 (8%)	**0.59 (57%)**	0.02 (2%)	-0.01 (-1%)	0.97	0.19
SR-OOA	0.14 (31%)	**0.23 (50%)**	0.05 (11%)	0.00 (0%)	-0.04 (-8%)	0.77	0.22
MO-OOA	**1.06 (71%)**	-0.13 (-9%)	0.14 (10%)	0.14 (10%)	0.01 (1%)	0.74	0.78
LO-OOA	**0.07 (29%)**	-0.07 (-28%)	0.06 (24%)	0.04 (15%)	-0.01 (-4%)	0.27	0.16
C-OOA	**0.48 (37%)**	-0.24 (-19%)	0.30 (23%)	0.26 (20%)	-0.02 (2%)	0.72	0.52

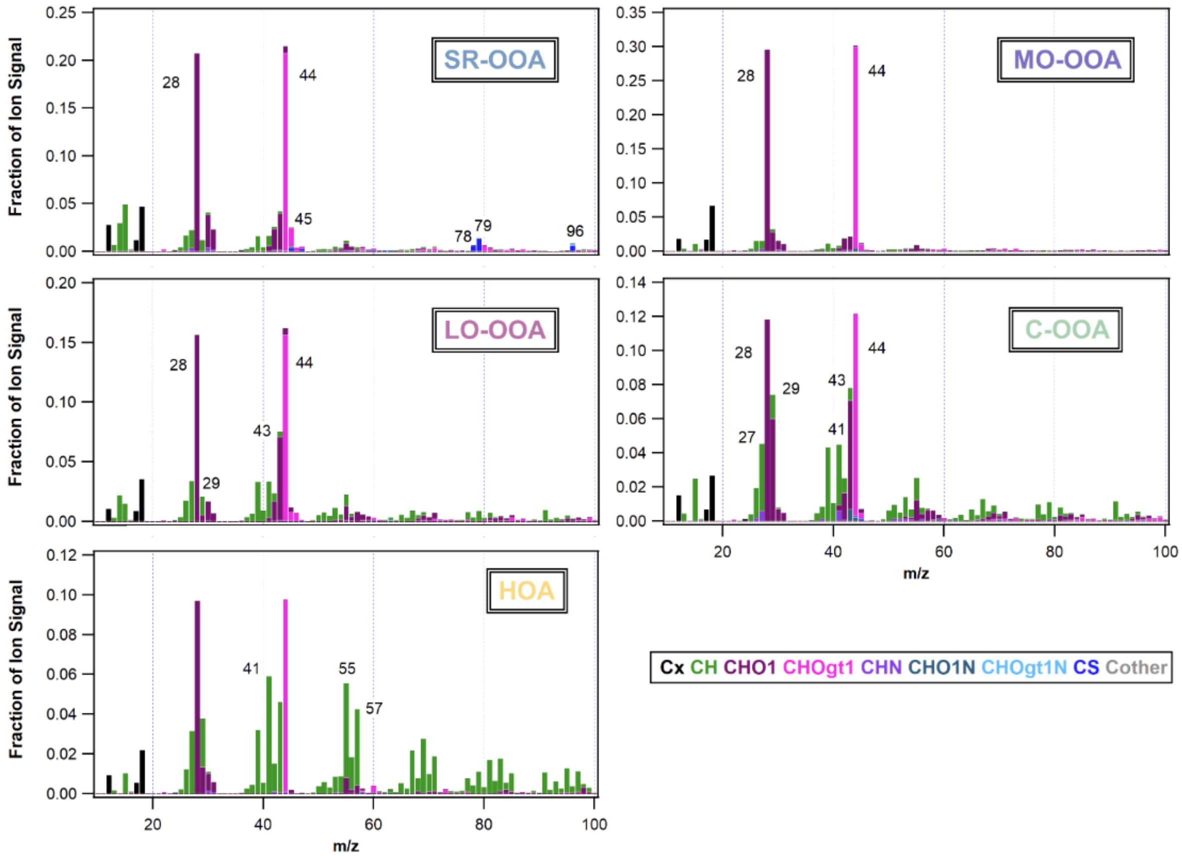

Figure S1: Mass spectra of factors resolved from PMF analysis of AMS NR HR-Org at Mt. Soledad. Factors include SR-OOA (top left), MO-OOA (top right), LO-OOA (middle left), C-OOA (middle right), and HOA (bottom left).

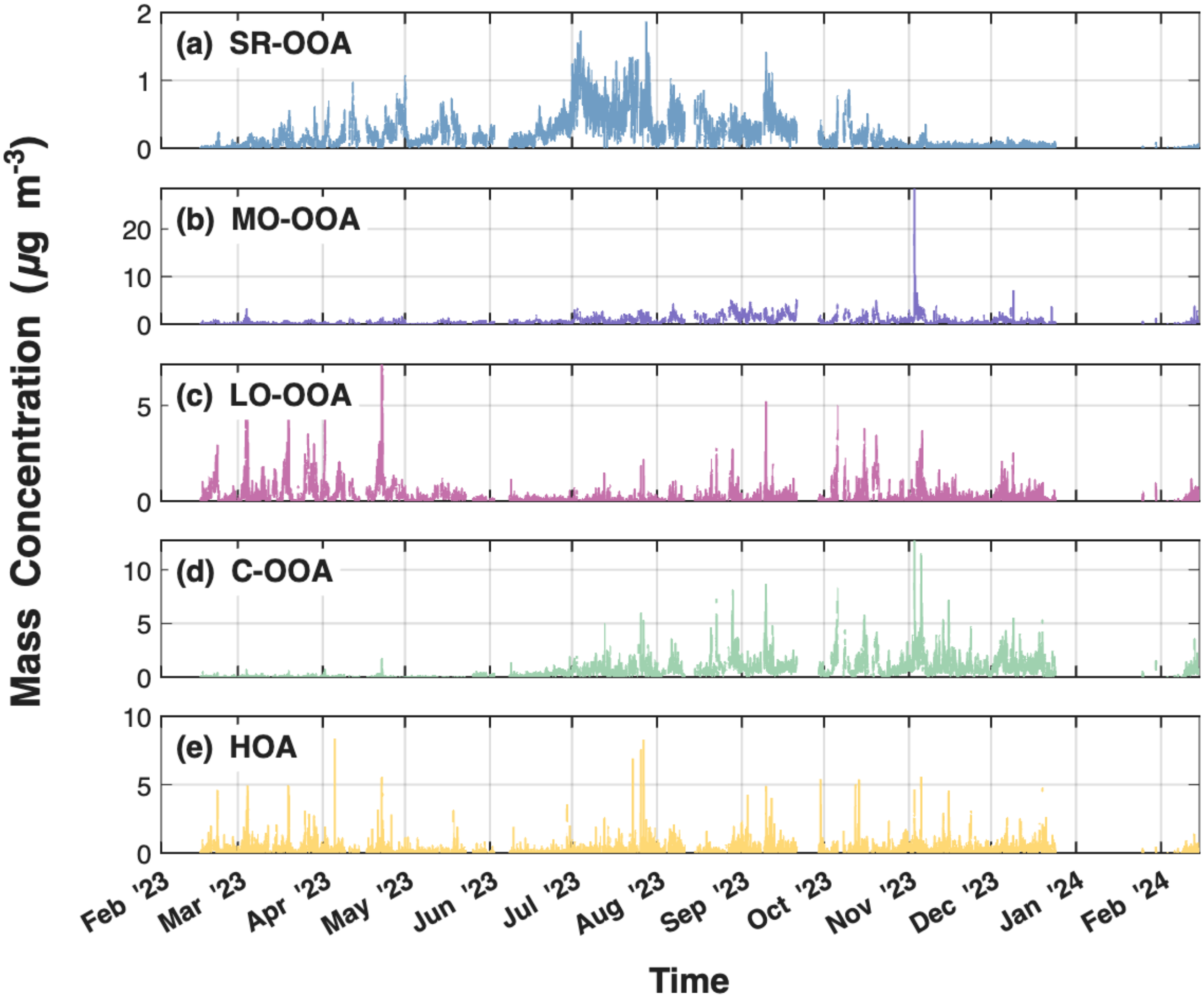

Figure S2: Time series of 5-minute ambient PMF factor mass concentrations at Mt. Soledad. Panels show (a) SR-OOA, (b) MO-OOA, (c) LO-OOA, (d) C-OOA, and (e) HOA. All measurements exclude times with particle number concentrations exceeding 8000 cm^{-3}.

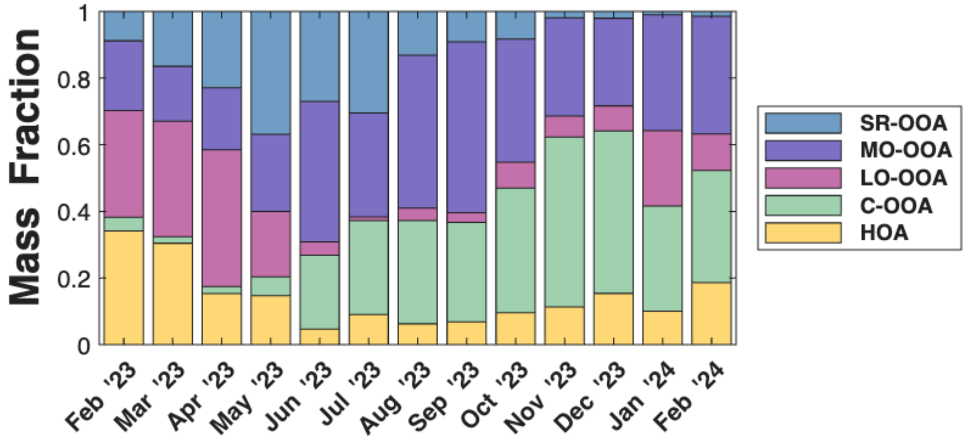

Figure S3: Monthly average mass fractions of AMS NR organic PMF factors at Mt. Soledad. All measurements exclude times with particle number concentrations exceeding 8000 cm^{-3}.

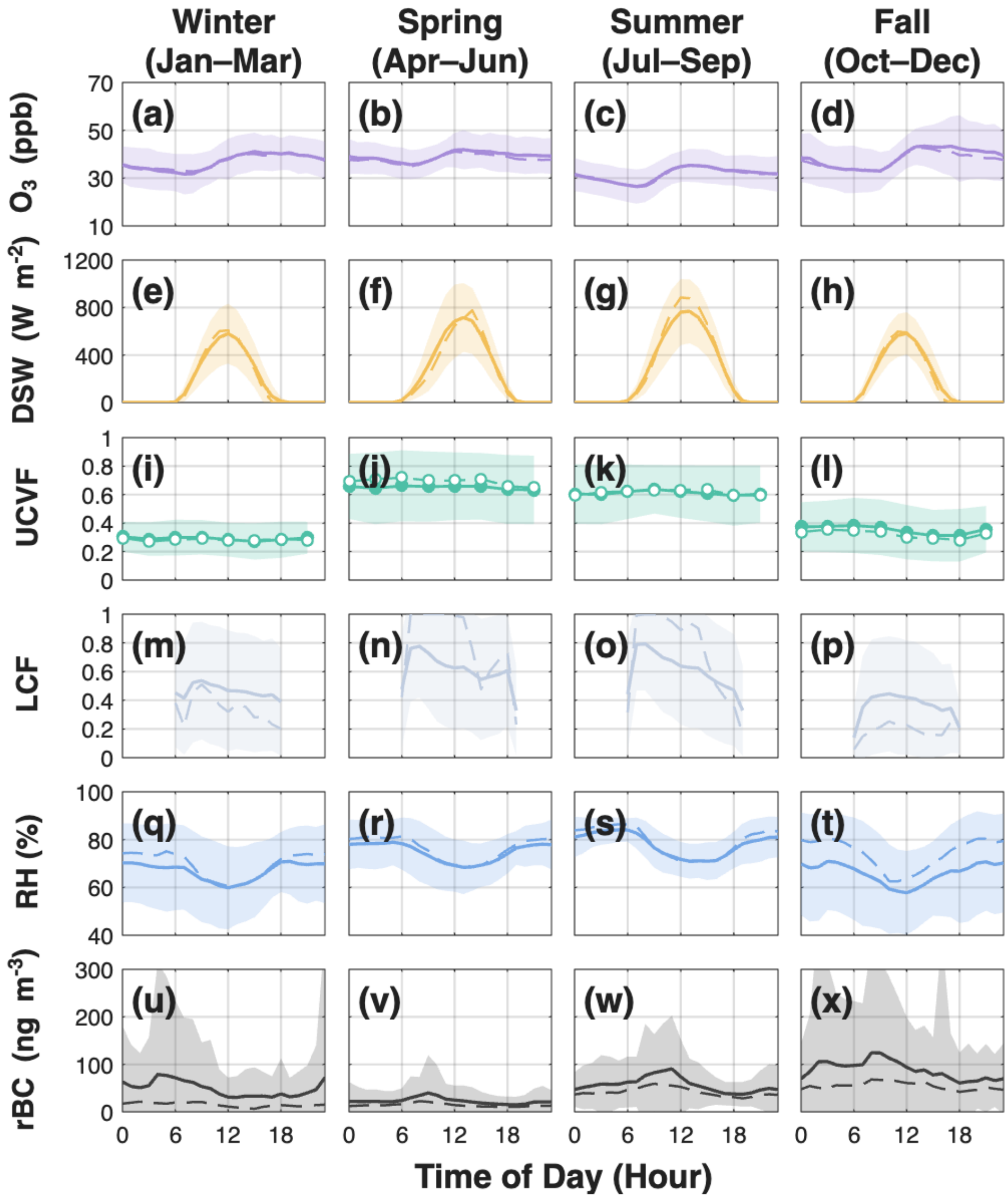

Figure S4: Seasonal diurnal patterns of O_3, DSW, UCVF, LCF, RH, and rBC at Mt. Soledad for all back-trajectories. O_3, DSW, LCF, RH, and rBC are shown in local time (PT), while UCVF is shown in UTC corresponding to its original 3-hour temporal resolution. O_3 and rBC exclude times with particle number concentrations exceeding 8000 cm^{-3}. The shaded area represents the standard deviation, the solid line represents the average, and the dashed line represents the median. For UCVF, filled markers indicate mean values and open markers indicate median values.

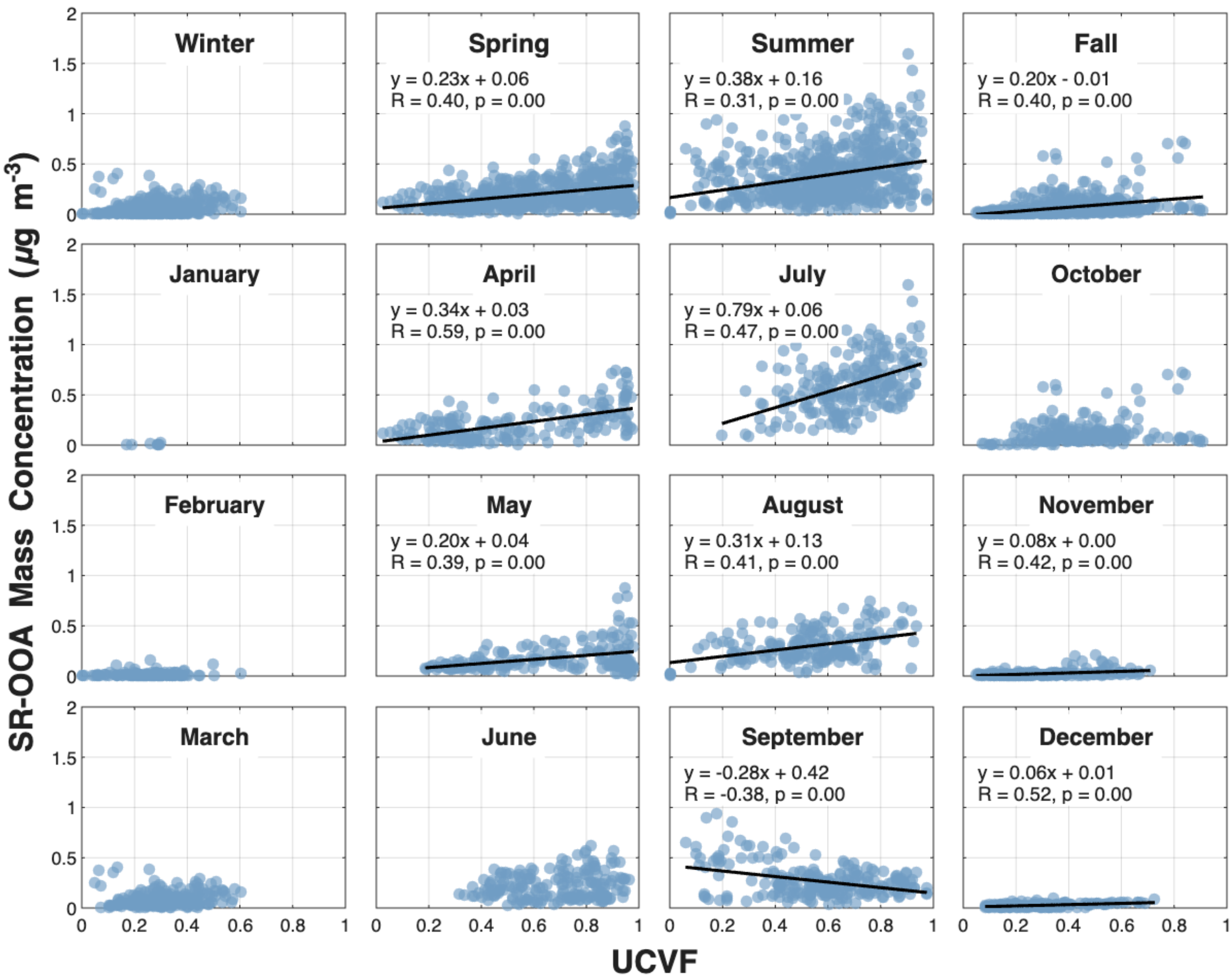

Figure S5: Monthly and seasonal scatterplots of SR-OOA mass concentration against UCVF. The top row shows seasonally combined data for winter, spring, summer, and fall, while the lower rows show individual monthly relationships within each season. Linear regression lines are shown only for relationships with $|R| \geq 0.25$ and $p \leq 0.05$, with the corresponding regression equation, Pearson correlation coefficient (R), and p-value indicated on the plots. Mass concentrations exclude times with particle number concentrations exceeding 8000 cm^{-3}.

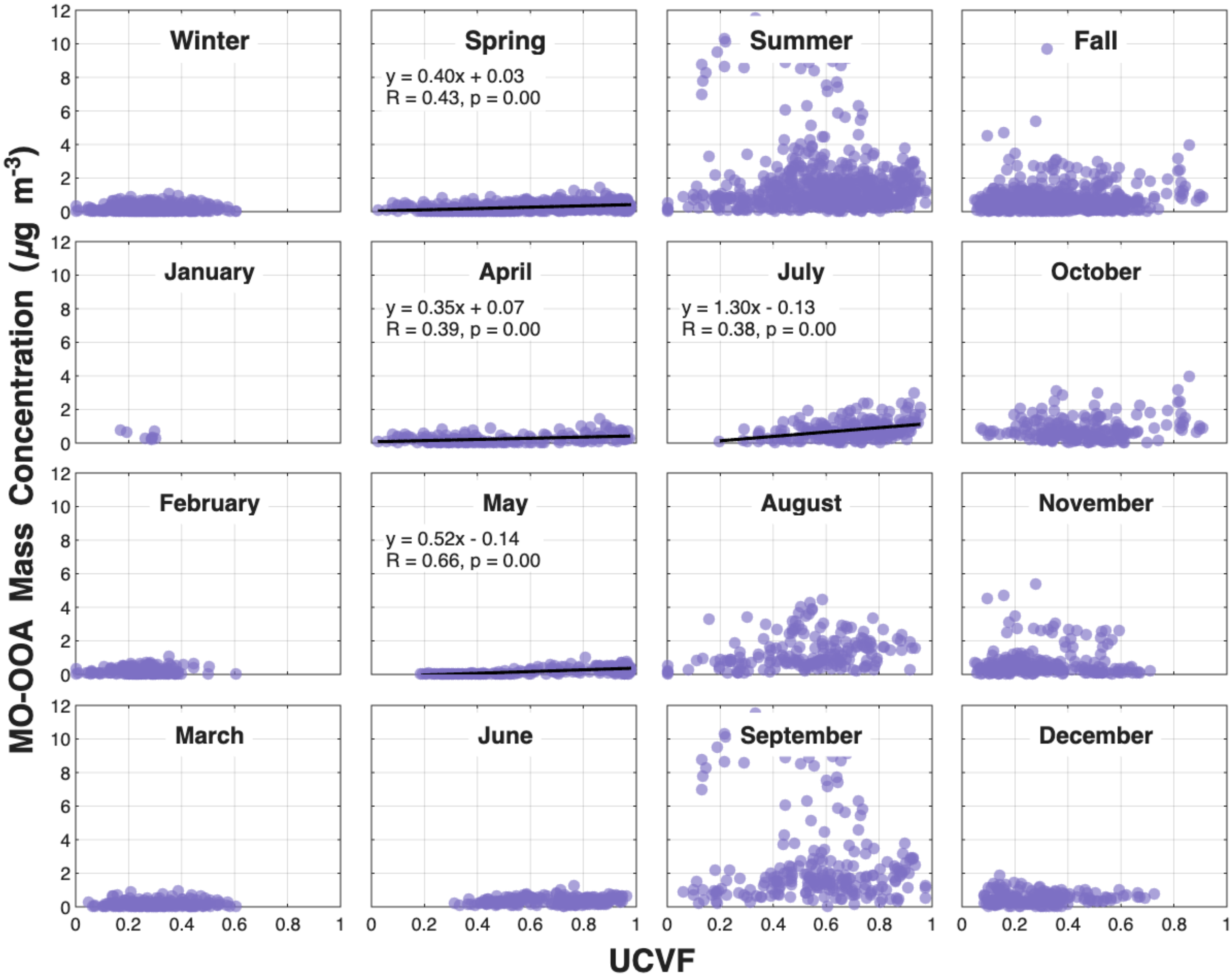

Figure S6: Monthly and seasonal scatterplots of MO-OOA mass concentration against UCVF. The top row shows seasonally combined data for winter, spring, summer, and fall, while the lower rows show individual monthly relationships within each season. Linear regression lines are shown only for relationships with |R| ≥ 0.25 and p ≤ 0.05, with the corresponding regression equation, Pearson correlation coefficient (R), and p-value indicated on the plots. Mass concentrations exclude times with particle number concentrations exceeding 8000 cm^{-3}.

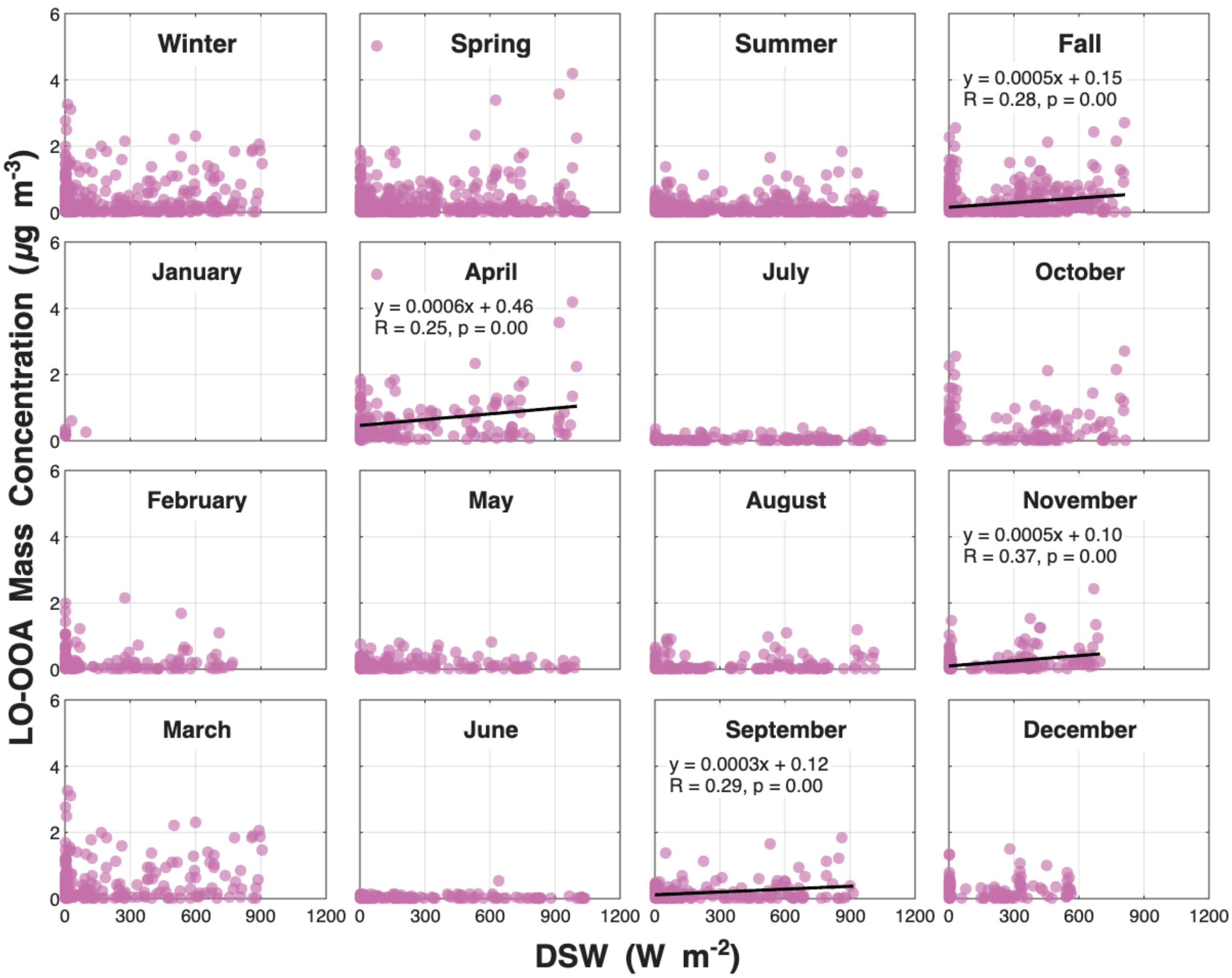

Figure S7: Monthly and seasonal scatterplots of LO-OOA mass concentration against DSW radiation. The top row shows seasonally combined data for winter, spring, summer, and fall, while the lower rows show individual monthly relationships within each season. Linear regression lines are shown only for relationships with |R| ≥ 0.25 and p ≤ 0.05, with the corresponding regression equation, Pearson correlation coefficient (R), and p-value indicated on the plots. Mass concentrations exclude times with particle number concentrations exceeding 8000 cm^{-3}.

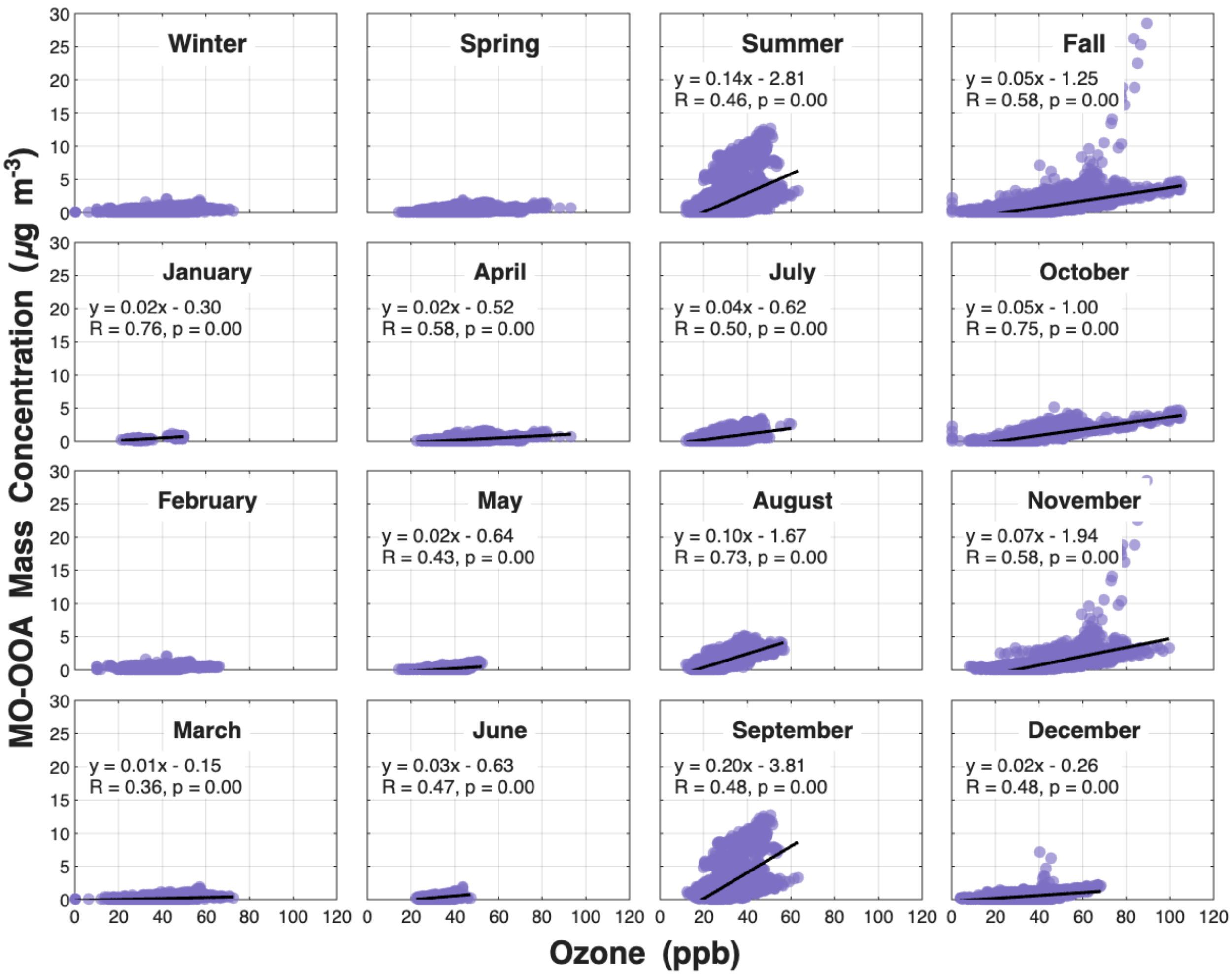

Figure S8: Monthly and seasonal scatterplots of MO-OOA mass concentration against ozone. The top row shows seasonally combined data for winter, spring, summer, and fall, while the lower rows show individual monthly relationships within each season. Linear regression lines are shown only for relationships with |R| ≥ 0.25 and p ≤ 0.05, with the corresponding regression equation, Pearson correlation coefficient (R), and p-value indicated on the plots. All measurements exclude times with particle number concentrations exceeding 8000 cm^{-3}.

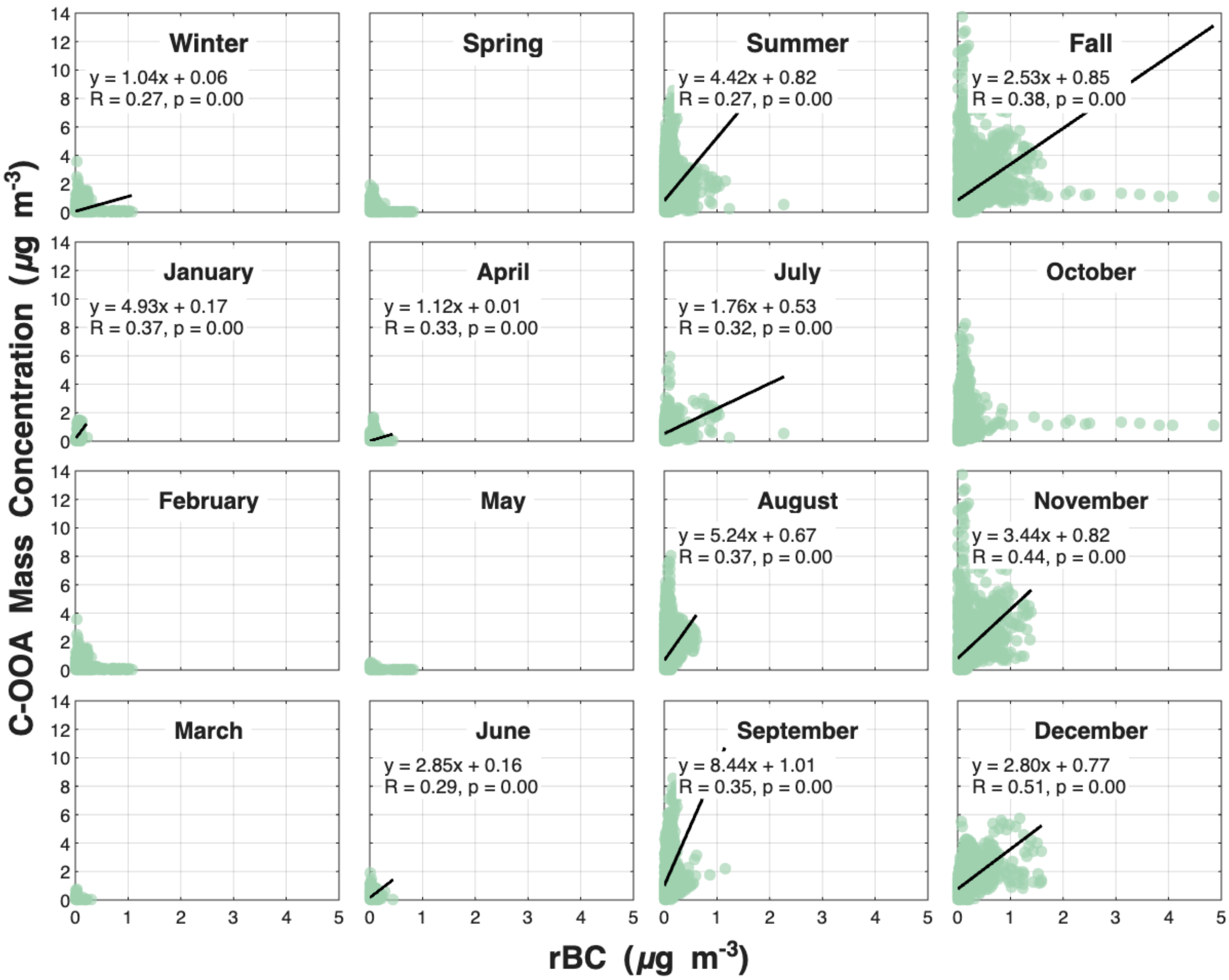

Figure S9: Monthly and seasonal scatterplots of MO-OOA mass concentration against ozone. The top row shows seasonally combined data for winter, spring, summer, and fall, while the lower rows show individual monthly relationships within each season. Linear regression lines are shown only for relationships with $|R| \geq 0.25$ and $p \leq 0.05$, with the corresponding regression equation, Pearson correlation coefficient (R), and p-value indicated on the plots. All measurements exclude times with particle number concentrations exceeding 8000 cm^{-3}.

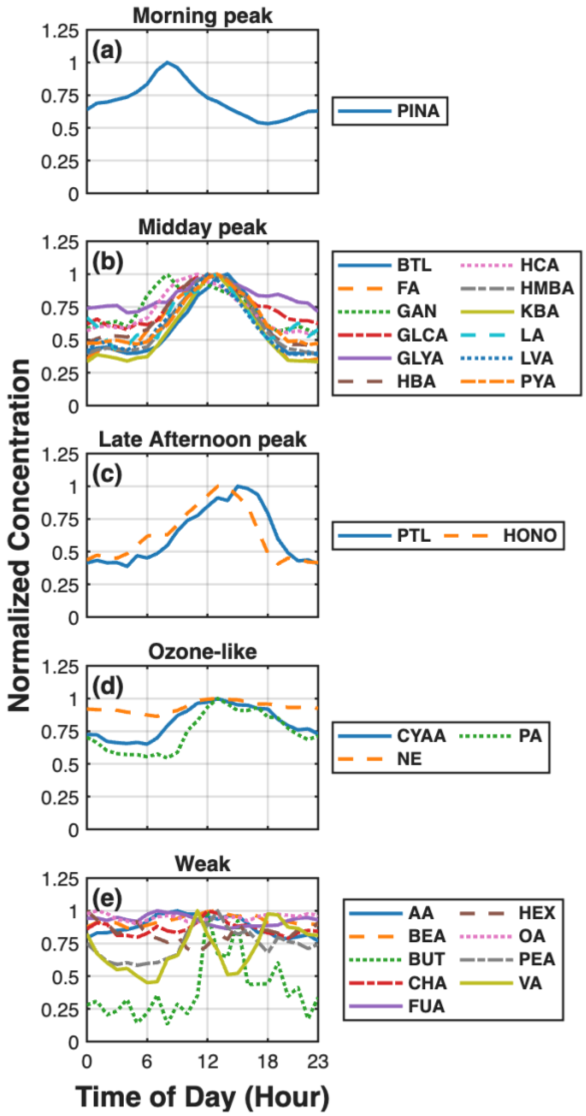

Figure S10: Normalized diurnal cycles of gas-phase CIMS organic acids at Mt. Soledad during EPCAPE shown in local time (PT). CIMS organic acids were grouped according to similarities in the shape and timing of their diurnal variability, including (a) morning peak, (b) midday peak, (c) late afternoon peak, (d) ozone-like behavior, and (e) no clear diurnal pattern. Each line represents the hourly mean concentration normalized to the maximum hourly mean concentration for that compound over the diurnal cycle. Data are grouped using abbreviated compound names defined in Table S#.

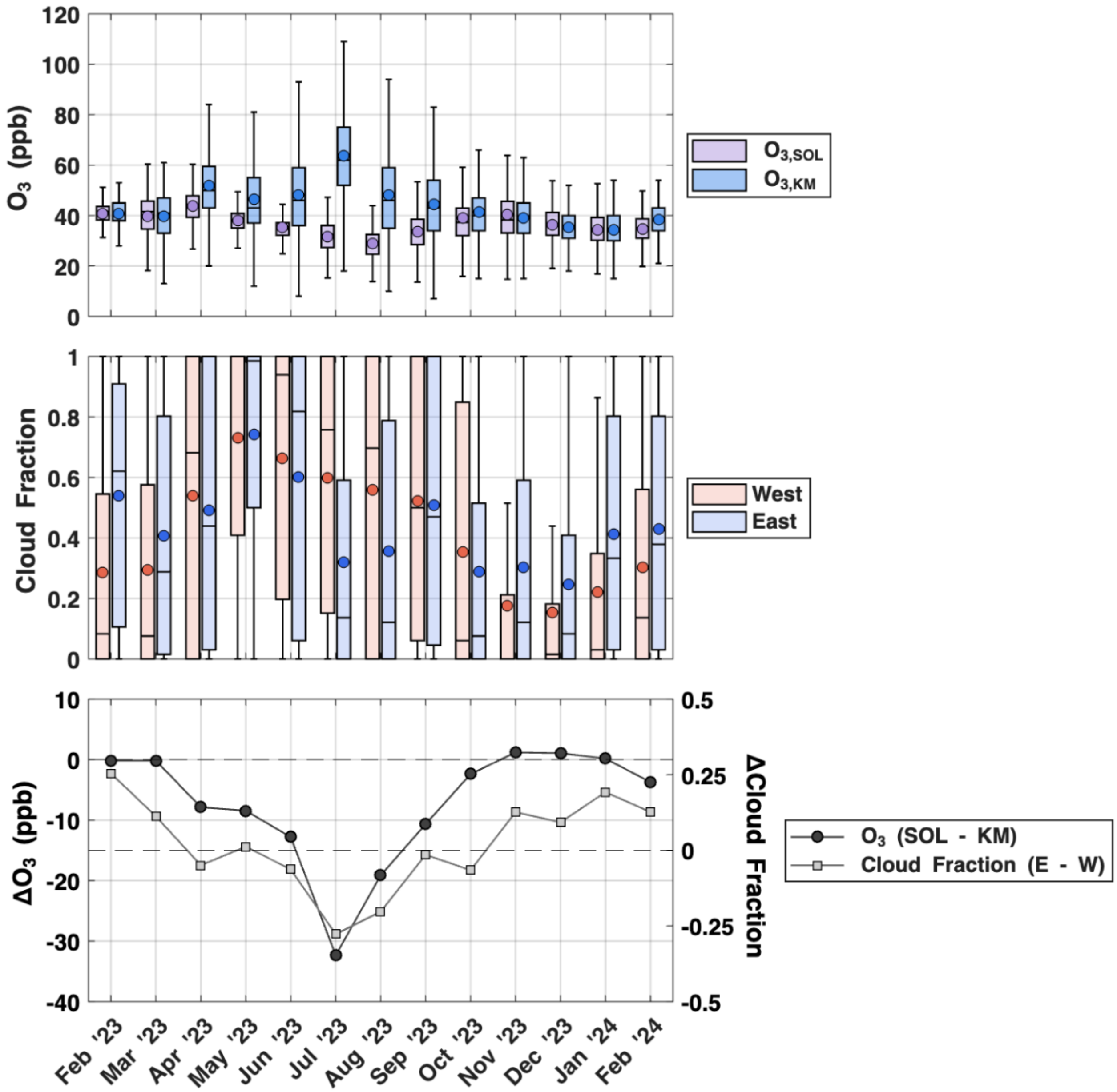

Figure S11: Monthly boxplots of (top) ozone concentrations measured at Mt. Soledad ($O_{3,SOL}$) and Kearny Mesa ($O_{3,KM}$), (middle) westward and eastward cloud fraction derived from SatCORPS satellite observations, and (bottom) the corresponding monthly differences in ozone concentration ($O_{3,SOL} – O_{3,KM}$; left axis) and cloud fraction (East − West; right axis). Colored shapes indicate monthly mean values, while boxplots indicate the interquartile range (IQR), with the middle line marking the median, the top edge representing the 75th percentile, and the bottom edge representing the 25th percentile. The whiskers extend to the maximum and minimum non-outlier values.

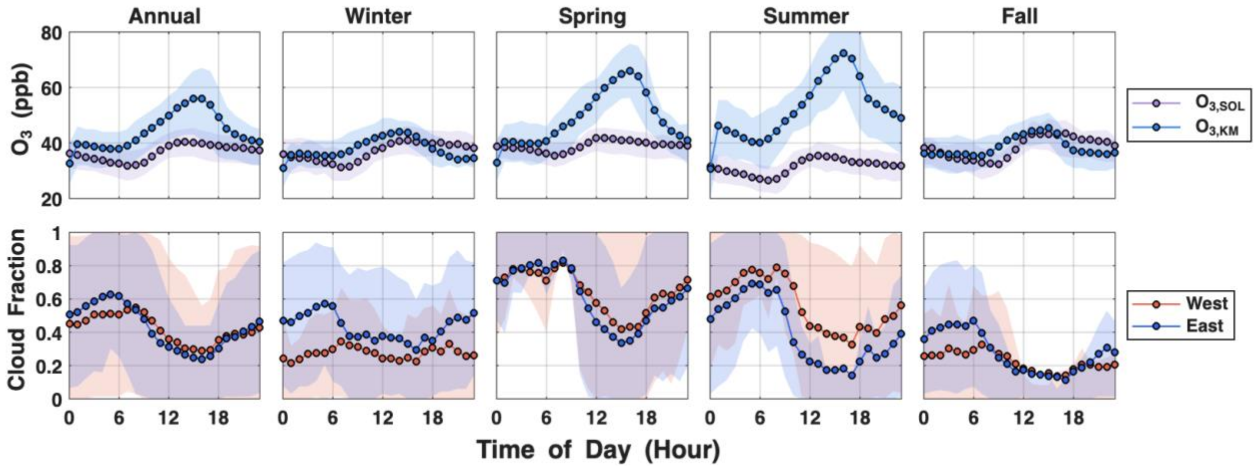

Figure S12: Diurnal patterns in (top) ozone concentrations measured at Mt. Soledad ($O_{3,SOL}$) and Kearny Mesa ($O_{3,KM}$) and (bottom) SATCORPS-derived westward and eastward cloud fraction in local time (PT). Columns correspond to annual conditions, winter, spring, summer, and fall from left to right. Solid lines represent mean diurnal cycles, while shaded regions represent ±1 standard deviation.

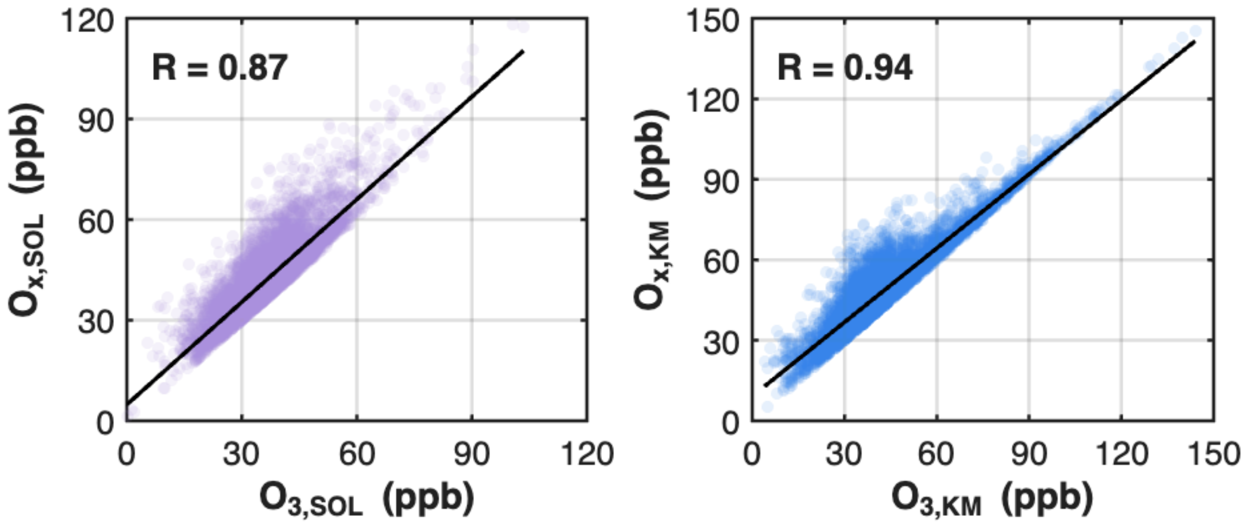

Figure S13: Scatterplots of ozone (O_3) against odd oxygen (O_X) concentration. The left panel shows ozone measured at Mt. Soledad ($O_{3,SOL}$) versus odd oxygen at Mt. Soledad ($O_{X,SOL}$), calculated as Soledad O_3 + Kearny Mesa NO_2. The right panel shows ozone ($O_{3,KM}$) measured at Kearny Mesa versus Kearny Mesa odd oxygen ($O_{X,KM}$), calculated as Kearny Mesa O_3 + Kearny Mesa NO_2. Solid black lines represent linear regressions. Pearson correlation coefficients (R) presented are all statistically significant ($p < 0.05$).

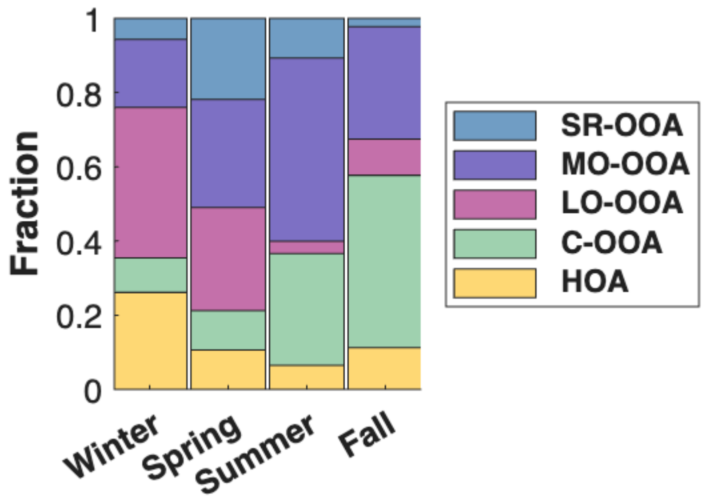

Figure S14. Seasonal average contributions of AMS NR organic PMF factors to O/C mass-weighted fraction of O/C from AMS NR organic PMF factors at Mt. Soledad. Contributions were calculated from factor-specific O/C values weighted by factor mass concentrations. All measurements exclude times with particle number concentrations exceeding 8000 cm^{-3}.

References.

Hayes, P. L., Ortega, A. M., Cubison, M. J., Froyd, K. D., Zhao, Y., Cliff, S. S., Hu, W. W., Toohey, D. W., Flynn, J. H., Lefer, B. L., Grossberg, N., Alvarez, S., Rappenglueck, B., Taylor, J. W., Allan, J. D., Holloway, J. S., Gilman, J. B., Kuster, W. C., De Gouw, J. A., ..., and Jimenez, J. L.: Organic aerosol composition and sources in Pasadena, California, during the 2010 CalNex campaign, Journal of Geophysical Research-Atmospheres, 118, 9233-9257, 10.1002/jgrd.50530, 2013.

Huang, D., Kong, L., Gao, J., Lou, S., Qiao, L., Zhou, M., Ma, Y., Zhu, S., Wang, H., Chen, S., Zeng, L., and Huang, C.: Insights into the formation and properties of secondary organic aerosol at a background site in Yangtze River Delta region of China: Aqueous-phase processing vs. photochemical oxidation, Atmospheric Environment, 239, 10.1016/j.atmosenv.2020.117716, 2020.

Li, J., Wang, G., Cao, J., Wang, X., and Zhang, R.: Observation of biogenic secondary organic aerosols in the atmosphere of a mountain site in central China: temperature and relative humidity effects, Atmospheric Chemistry and Physics, 13, 11535-11549, 10.5194/acp-13-11535-2013, 2013.

Li, J., Cao, L., Gao, W., He, L., Yan, Y., He, Y., Pan, Y., Ji, D., Liu, Z., and Wang, Y.: Seasonal variations in the highly time-resolved aerosol composition, sources and chemical processes of background submicron particles in the North China Plain, Atmospheric Chemistry and Physics, 21, 4521-4539, 10.5194/acp-21-4521-2021, 2021.

Liu, S., Day, D. A., Shields, J. E., and Russell, L. M.: Ozone-driven daytime formation of secondary organic aerosol containing carboxylic acid groups and alkane groups, Atmospheric Chemistry and Physics, 11, 8321-8341, 10.5194/acp-11-8321-2011, 2011.

Rogers, M., Joo, T., Hass-Mitchell, T., Canagaratna, M., Campuzano-Jost, P., Sueper, D., Tran, M., Machesky, J., Roscioli, J., Jimenez, J., Krechmer, J., Lambe, A., Nault, B., and Gentner, D.: Humid Summers Promote Urban Aqueous-Phase Production of Oxygenated Organic Aerosol in the Northeastern United States, GEOPHYSICAL RESEARCH LETTERS, 52, 10.1029/2024GL112005, 2025.

Sun, Y., Du, W., Fu, P., Wang, Q., Li, J., Ge, X., Zhang, Q., Zhu, C., Ren, L., Xu, W., Zhao, J., Han, T., Worsnop, D., and Wang, Z.: Primary and secondary aerosols in Beijing in winter: sources, variations and processes, Atmospheric Chemistry and Physics, 16, 8309-8329, 10.5194/acp-16-8309-2016, 2016.

Wood, E., Canagaratna, M., Herndon, S., Onasch, T., Kolb, C., Worsnop, D., Kroll, J., Knighton, W., Seila, R., Zavala, M., Molina, L., DeCarlo, P., Jimenez, J., Weinheimer, A., Knapp, D., Jobson, B., Stutz, J., Kuster, W., and Williams, E.: Investigation of the correlation between odd oxygen and secondary organic aerosol in Mexico City and Houston, ATMOSPHERIC CHEMISTRY AND PHYSICS, 10, 8947-8968, 10.5194/acp-10-8947-2010, 2010.

Xiao, Y., Hu, M., Zong, T., Wu, Z., Tan, T., Zhang, Z., Fang, X., Chen, S., and Guo, S.: Insights into aqueous-phase and photochemical formation of secondary organic aerosol in the winter of Beijing, Atmospheric Environment, 259, 10.1016/j.atmosenv.2021.118535, 2021.

Xu, W., Han, T., Du, W., Wang, Q., Chen, C., Zhao, J., Zhang, Y., Li, J., Fu, P., Wang, Z., Worsnop, D., and Sun, Y.: Effects of Aqueous-Phase and Photochemical Processing on Secondary Organic Aerosol Formation and Evolution in Beijing, China, Environmental Science and Technology, 51, 762-770, 10.1021/acs.est.6b04498, 2017.

Yao, D., Guo, H., Lyu, X., Lu, H., and Huo, Y.: Secondary organic aerosol formation at an urban background site on the coastline of South China: Precursors and aging processes, Environmental Pollution, 309, 10.1016/j.envpol.2022.119778, 2022.

Zhan, B., Zhong, H., Chen, H., Chen, Y., Li, X., Wang, L., Wang, X., Mu, Y., Huang, R., George, C., and Chen, J.: The roles of aqueous-phase chemistry and photochemical oxidation in oxygenated organic aerosols formation, Atmospheric Environment, 266, 10.1016/j.atmosenv.2021.118738, 2021.